JOURNAL OF CATALYSIS 149, 300–306 (1994)

Mechanism of COS Hydrolysis on Alumina

P. E. Hoggan,* A. Aboulayt,* A. Pieplu,* P. Nortier,† and J. C. Lavalley*,[1]

*Laboratoire Catalyse et Spectrochimie, URA CNRS DO 414, ISMRA Université de Caen, 6 Boulevard du Maréchal Juin, 14050 Caen Cédex, and †Centre de Recherche Rhône-Poulenc, 52 Rue de la Haie Coq, 93308 Aubervilliers Cédex, France

Received January 24, 1994; revised May 4, 1994

COS adsorption was studied by infrared spectroscopy on γ-alumina activated at various temperatures. Evidence for hydrogen thiocarbonate (HTC) species was provided from the interaction with monodentate OH groups, the most basic. On highly activated samples, additional weakly chemisorbed species occurred through the interaction between COS and Lewis acid or basic sites. HTC species were shown to play the role of intermediates in the COS hydrolysis reaction. Conversely, studies at low temperature showed that hydrogen carbonate species resulted from the readsorption of CO_2, a reaction product. Quantum chemistry calculations corroborated the infrared results and provided complementary information regarding the hydrolysis mechanism. In particular, the cyclic geometry of the transition state was found to occur through a nearly regular hexagonal configuration. Moreover, the activation barriers for HTC formation and hydrolysis were calculated and found to be similar.

INTRODUCTION

Natural or industrial gases may contain high percentages of sulfur compounds, especially hydrogen sulfide. The Claus reaction is that most frequently used to transform H_2S into harmless compounds. In the course of the thermal step of this process, formation of undesirable products is observed, notably carbon disulfide and oxysulfide (1) which must be removed from the effluent. One of the most effective methods of achieving this is hydrolysis.

Little fundamental work on the hydrolysis of COS on metal oxides has been published with the exception of that on alumina. Namba and Shiba (2) have shown that the active sites on alumina are the basic sites. Zdražil (3) reported that oxygen is a poison toward this reaction on alumina and sodium aluminates. George (4, 5) confirmed that basicity and rate of COS hydrolysis vary in the same direction, using Co–Mo catalysts supported on sodium Chromosorb. Akimoto and Dalla Lana (6) initially suggested that the active sites were reducing sites. However, from experiments carried out on sodium aluminates and results obtained by ammonia, pyridine, or acetic acid addition, they conclude that the basic sites are essential for the reaction and suggest competitive adsorption of COS and H_2O (7).

In a recent article (8) we showed zirconia to be more active than titanium oxide (anatase). In addition, the presence of sulfur dioxide reversibly poisons the COS hydrolysis reaction due to competitive adsorption of these two compounds on the basic hydroxyl sites (8, 9). Finally, the sulfation of oxides leads to irreversible deactivation explained by the creation of Brønsted acid sites to the detriment of basic sites (8, 9).

The present work is devoted in particular to the determination of the mechanism of COS hydrolysis on alumina. The experimental study was made using infrared spectroscopy and the proposed mechanism then detailed by quantum chemical calculations.

METHODS

The alumina used was a standard γ-Al_2O_3 from Rhône-Poulenc (10). Its surface area was 207 $m^2\ g^{-1}$. Samples were used as self-supporting wafers of ca. 10 mg cm^{-2}, treated *in situ* by evacuation at different temperatures. Then a measured amount (350 μmol g^{-1}) of COS (Prodair, purity 96%) was introduced either at room temperature (RT) or at 200 K. IR spectra were recorded using a Nicolet MX-1 FTIR spectrometer with a resolution of 2 cm^{-1}.

Quantum chemistry calculations were carried out using the adapted GEOMOS package (11) written by one of us. This permits study of a reaction pathway for adsorbed species on metals and metal oxides as substrates at the semiempirical level. A size-consistent embedded cluster method is used. The GEOMOS codes have been optimized and tuned for running on IBM RS 6000 machines.

The theoretical basis of our calculations involves various innovations described in detail elsewhere (11–14). The choice of semiempirical or *ab initio* calculations is simply dictated by the size of the systems of interest.

In the present work at the semiempirical level a new

[1] To whom correspondence should be addressed.

0021-9517/94 $6.00

MNDO Hamiltonian in an spd basis of Slater-type orbitals is used (15). Full geometry optimisations were carried out on a supermolecule containing the adsorbate and an active site with several-unit mesh of the substrate embedded initially in a perfectly periodic lattice of alumina. This is done using an extension of the GEOMOS program (11). The program calculates the perturbed density matrix for the system using the total electronic potential calculated from the Green matrix (12–14). The codes have been run on IBM 340 and 355 powerstations.

Evaluation of the bielectronic integrals which must, of necessity, use the spherical tensor approach, both to include the sulfur *d* orbitals and to provide reliable electronic spectra, is detailed in a previous paper (15).

For all the structures calculated, a geometry optimization was carried out using a conjugate gradient method of energy minimization with respect to atomic Cartesian coordinates [our adapted BFGS algorithm (11, 12)].

The environment is divided into two subsystems. First, a reactive site is considered as part of the supermolecule with the adsorbate and optimized according to the above method. Second, the rest of the substrate is treated as a perfect cubic crystal lattice and surface Bloch functions (so-called Tamm states). These functions are expressed in an LCAO of Slater-type orbitals or, equivalently, the corresponding Bessel functions (12).

The molecular orbitals and Bloch functions are used to initialize the Green matrix of the system working in the potential framework. This use of the electronic potential renders the method entirely size consistent. Previous calculations show that at least 12–14 substrate atoms should nevertheless be taken to construct the substrate active site (12). The present calculations took 30 substrate atoms into account for the adsorbate–substrate supermolecule. An SCRF calculation completes the initialization by fixing the values of the coefficients required in the direct sum of the molecule and solid Green matrices (12). The adduct system Green matrix is perturbed directly using the series described in Refs. (12–14). The final density matrix is subsequently obtained by inverse Fourier transformation. The energy and its derivatives are then evaluated.

This method incorporates many electronic configurations via the potential and accounts for at least four-fifths of the correlation energy.

The reaction pathway is followed by identifying internal coordinates which represent the progress of the reaction. These are taken as the reaction coordinate which is increased in a series of small steps. At each new value, an optimization minimizes the total energy with respect to all the other internal coordinates defining the supermolecule. The height of the saddle point on this pathway compared with the starting point gives an estimation of the activation barrier.

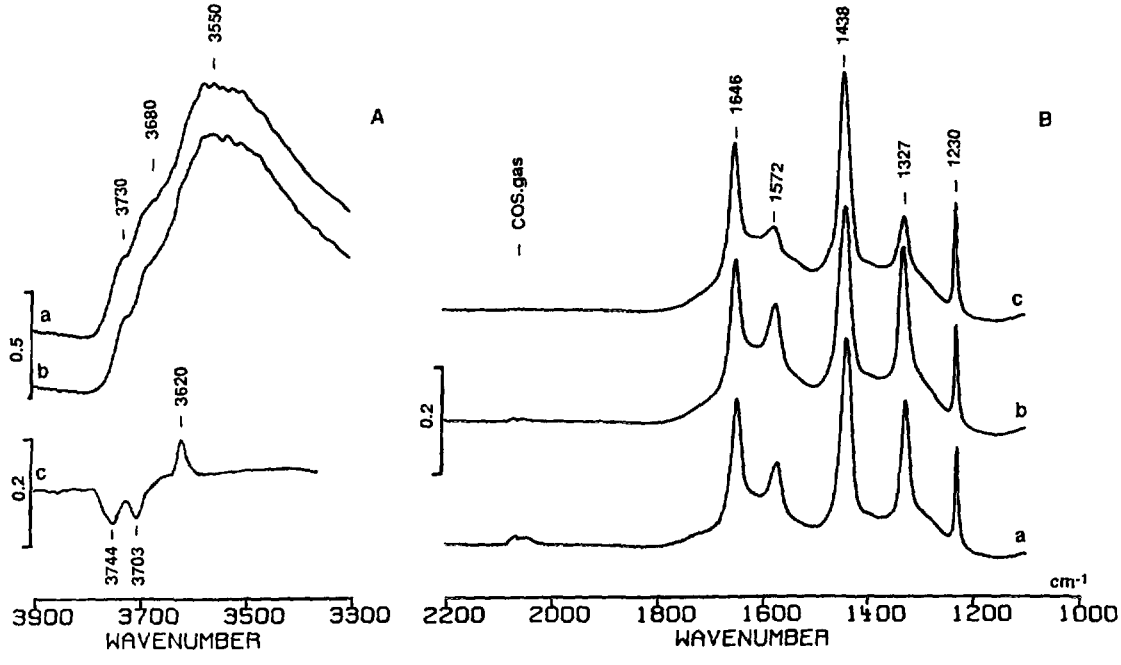

FIG. 1. IR spectra resulting from COS adsorption at room temperature (RT) on Al_2O_3 evacuated at RT (A) ν(OH) bands (a) before and (b) after COS introduction (contact time: 2 h); (c) difference in spectra (b) − (a). (B) Bands due to COS adsorption after contact times of (a) 5 min and (b) 2 h at RT and 15 min at 323 K (c).

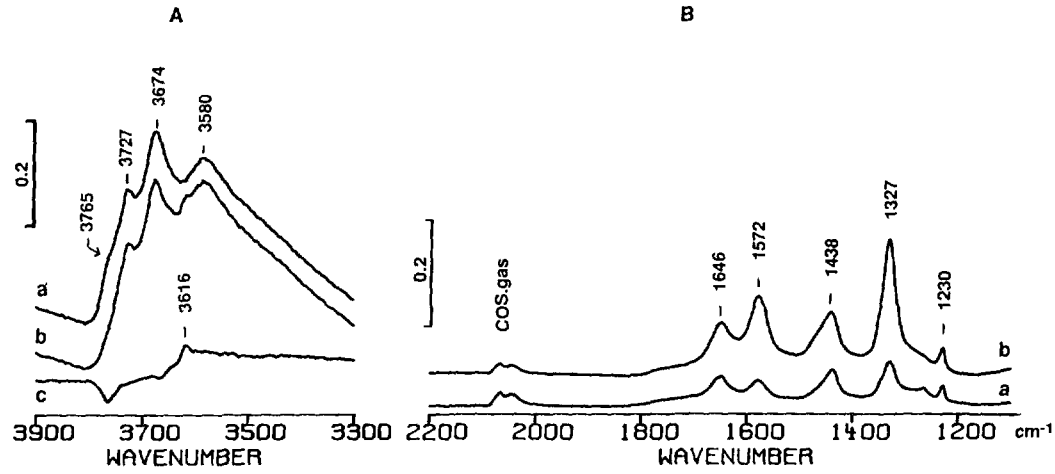

FIG. 2. IR spectra resulting from COS adsorption at RT on Al_2O_3 evacuated at 573 K. See legend to Fig. 1.

RESULTS AND DISCUSSION

A. Infrared Spectroscopy

The spectrum of alumina evacuated at room temperature presents a broad band centered around 3550 cm^{-1} due to hydrogen-bonded hydroxyl groups, accompanied by shoulders near 3680 and 3730 cm^{-1} indicating the presence of free hydroxyl groups (Fig. 1). The addition of COS gives rise to bands at 1646, 1438, and 1230 cm^{-1} characteristic of hydrogen carbonate species (16) and to two other bands, at 1572 and 1327 cm^{-1}, corresponding to species denoted by *X*, with increasing intensity as a function of time. Note that the band due to gas-phase COS, centered near 2060 cm^{-1}, is always weak and tends to disappear with time (Fig. 1). It completely vanishes when the alumina is heated to 323 K. We then observe an increased intensity of the bands due to the hydrogen carbonate species at the expense of those due to species *X*. This suggests that species *X* plays the role of an intermediate. In the ν(OH) frequency range, subtracted spectra show the appearance of a band at 3620 cm^{-1} due to hydrogen carbonate species, whereas both bands at 3744 and 3703 cm^{-1} decrease in intensity.

The spectrum of alumina evacuated at 523 K essentially presents three OH bands at 3727, 3674, and 3580 cm^{-1} (Fig. 2), the last being far less intense than after evacuation of alumina at room temperature. We note the presence of a shoulder at 3765 cm^{-1}. Introduction of COS gives rise to hydrogen carbonate formation and species *X*. The

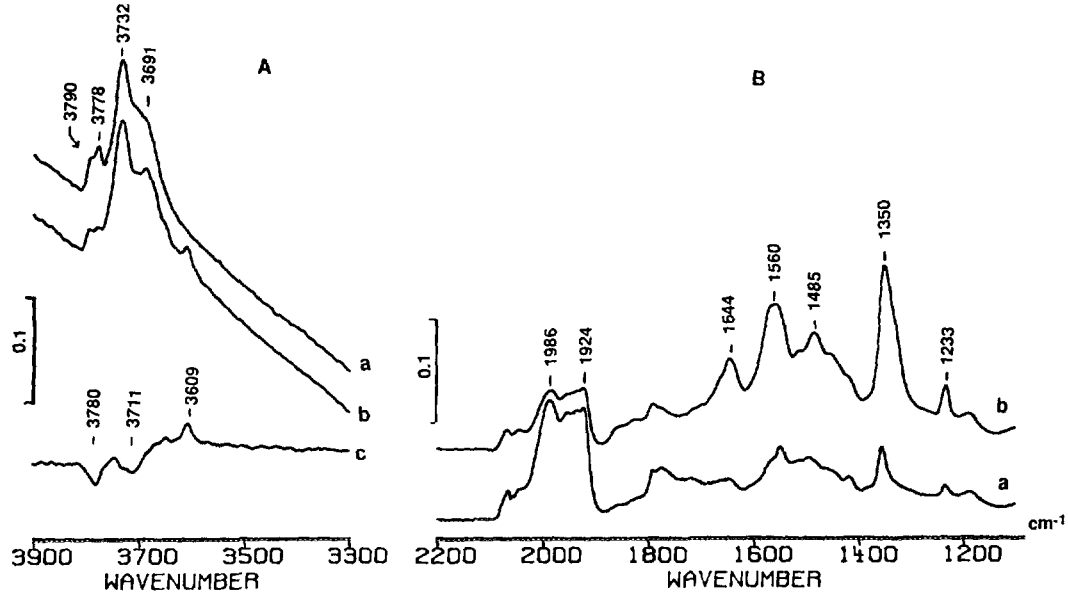

FIG. 3. IR spectra resulting from COS adsorption at RT on Al_2O_3 evacuated at 873 K. See legend to Fig. 1.

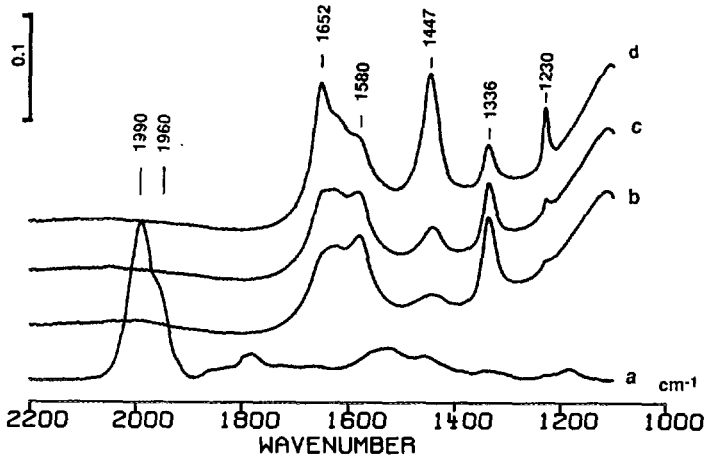

FIG. 4. IR spectra resulting from COS adsorption at RT on Al_2O_3 evacuated at 1123 K, after (a) 15 min of contact, followed by H_2O addition at RT, the contact times being (b) 2 min, (c) 30 min, and (d) 12 h.

number of the latter increases with time such that the intensities of the characteristic bands become greater than those of the hydrogen carbonate species. The quantity of residual gas-phase COS is greater than that persisting in contact with alumina evacuated at room temperature. The difference in the spectra in the hydroxyl region shows a net reduction in intensity of the shoulder at 3765 cm^{-1} on addition of COS. The OH band appearing at 3616 cm^{-1} is due to hydrogen carbonate species.

The spectrum of alumina evacuated at 873 K presents free OH bands at 3790 (shoulder), 3778, 3732, and 3691 cm^{-1} (shoulder) (Fig. 3). Introduction of COS essentially gives rise after 5 min to a range of peaks between 1900 and 2000 cm^{-1}, with maxima at 1986, 1950, and 1924 cm^{-1} due to slightly perturbed COS species. With time, species *X* and the hydrogen carbonates appear clearly but the band intensities of the latter are always very low. Note that the spectrum of the latter is more complex, in agreement with results obtained by adsorbing CO_2 on alumina activated at high temperature (16). The difference in the spectra shows the preferential disappearance of the hydroxyl groups giving rise to the band at 3780 cm^{-1}.

The alumina evacuated at 1123 K presents practically no residual hydroxyl groups. The introduction of COS gives rise only to the scarcely perturbed COS species (bands at 1990 accompanied by a shoulder at 1960 cm^{-1}). In particular, the intensities of the *X* and hydrogen carbonate bands always remain very low even after 15 min of contact with the alumina (Fig. 4). Addition of water suppresses the weakly perturbed COS species, whereas the bands due to the species denoted by *X* are prevalent just after addition of water; then bands due to these species decrease with time at the expense of those due to hydrogen carbonate species.

This leads us to conclude that surface hydroxyl groups or water is necessary to form species *X*. An experiment performed on alumina exchanged by D_2O at 523 K and then evacuated at this temperature shows that the wavenumbers of the bands due to species *X* are unaltered by OH–OD substitution. Only the intensity of the band at 1232 cm^{-1} attributed to the δ (OH) vibration of hydrogen carbonate species is affected, as expected (17).

Finally, COS was adsorbed at 200 K on alumina evacuated at 523 K. Apart from physisorbed COS (band at 2040 cm^{-1}), we observe species *X* formation without formation of hydrogen carbonate species (Fig. 5). On the other hand, we note the appearance of a very sharp band due to physisorbed CO_2 at 2342 cm^{-1}. It disappears on raising the temperature to room temperature, the hydrogen carbonate species increasing concomitantly.

B. Interpretation of IR Results

COS is a polar molecule with the following partial charges calculated using MNDO/2 (15):

$$\overset{-0.27}{O} = \overset{+0.11}{C} = \overset{+0.16}{S}$$

Slightly perturbed COS species. On very dehydroxylated alumina (activated at 1123 K), two bands are observed at 1990 and 1960 cm^{-1}. They correspond to scarcely perturbed COS species; the interaction involves Lewis sites, either very weakly acid or basic. We can invoke the following species:

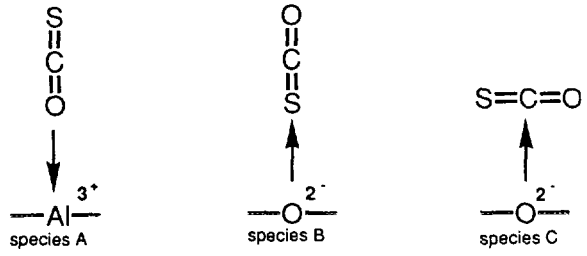

In a previous article (9), we reported that adsorption of COS on sulfated alumina gave rise only to the physisorbed species characterized by the band at 1997 cm^{-1}. Having shown elsewhere that sulfating alumina poisoned the basic sites and slightly increased the strength of Lewis acid sites (18), we conclude that the band at 1990–1997 cm^{-1} characterizes the formation of species A. The other band observed on pure alumina at 1960 cm^{-1} can be assigned to species B and/or C, and apparently involves very weakly basic sites. The presence of very basic O^{2-} sites should lead to the formation of thiocarbonate $(CO_2S)^{2-}$ species which we could not detect by adsorption of COS on very dehydroxylated alumina.

Note that CO_2 also forms species analogous to A on alu-

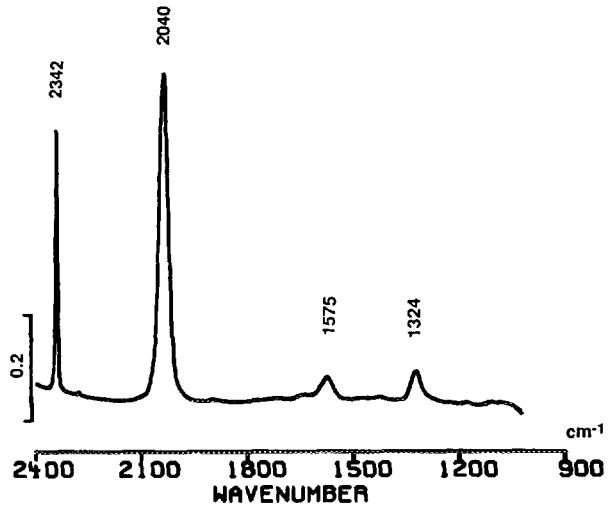

FIG. 5. IR spectra resulting from COS adsorption at 200 K on Al_2O_3 evacuated at 523 K (contact time: 30 min).

mina, referred to as "linear CO_2." A higher wavenumber than for the gas phase corresponds to these species [$\nu_a(CO_2)$ = 2349 cm^{-1}]; the greater the surface Lewis acidity, the higher the wavenumber (19). Conversely, the wavenumber ν(CO) of type A species in the COS case is lower than that observed for COS in the gas phase (ν_3 = 2062 cm^{-1}). This result can easily be explained by taking into account the electron transfer from the oxygen to the Lewis acid. In the case of the symmetric molecule CO_2, this transfer reduces the electron density of bond 1 and increases that of bond 2:

$$\overset{\quad 1 \quad 2}{Al^{3+} \leftarrow O = C = O}$$

This results in increasing the CO frequency (bond 2). In the COS case, this transfer reduces the electron density of the CO bond and explains the shift toward lower wavenumber. Conversely, it should increase the ν(CS) wavenumber (853 cm^{-1}) which cannot be detected due to the lack of transparency of the sample below 1000 cm^{-1}.

Species X. Species *X* is characterized by two bands near 1575 and 1325 cm^{-1}. In a previous article (20) we showed that these two bands appeared when H_2S containing traces of CO_2 is adsorbed on alumina. Their wavenumber is altered by isotopic substitution ^{12}C–^{13}C or ^{16}O–^{18}O in CO_2 but is invariant to H–D substitution in H_2S (21). This result is confirmed by the present study: the adsorption of COS on alumina exchanged by D_2O gives rise to the same bands at 1575 and 1325 cm^{-1}.

Species *X* had tentatively been identified as being of thiocarbonate type (20). This study, however, shows that their formation requires the presence of surface hydroxyl groups. We therefore prefer to assign the two bands at 1575 and 1325 cm^{-1} to a species of hydrogen thiocarbonate (HTC) type by analogy with the hydrogen carbonate (HC) species formed by CO_2 adsorption on basic alumina hydroxyls. Several HTC structures can be written according to whether the proton is bound to the sulfur atom or the oxygen, among them the following (bidentate species assumed):

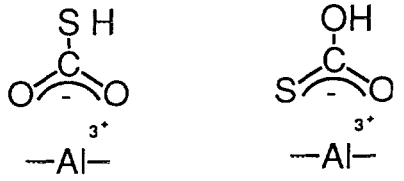

Type I (HTC species) Type II (HTC species)

The δ(OH) band of the HC species, situated near 1230 cm^{-1}, is sensitive to H–D substitution (17). It should be the same for the type II HTC species. However, the two bands at 1575 and 1325 cm^{-1} persist when adsorbing COS on the previously deuterated alumina substrate. We thus favor the type I structure, although no ν(SH) band at around 2600–2500 cm^{-1} has been detected. Note, however, that this band is very weak in general (22) which explains its nondetection.

We have shown (23) that CO_2 inserts itself into the S–Al bond of CH_3S species adsorbed on alumina to give

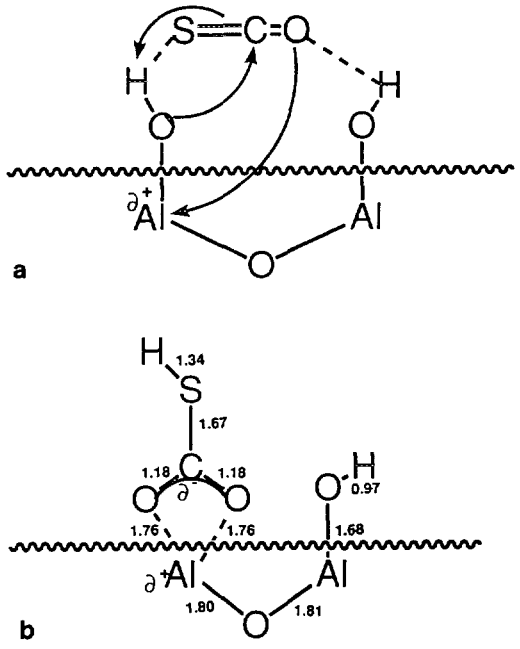

FIG. 6. COS hydrolysis mechanism established by quantum chemical calculations (in-plane projection, distances in Ångstroms). (a) Initial step, (b) HTC species formation.

methylthiocarbonate species. Following similar reaction pathways, type I HTC species can be formed from COS and basic alumina OH groups (in particular, monodentate hydroxyls).

Mechanism of the hydrolysis reactions. On the surface the reaction can proceed via two pathways according to whether the HTC species reacts with a proton (pathway I) or water (pathway II):

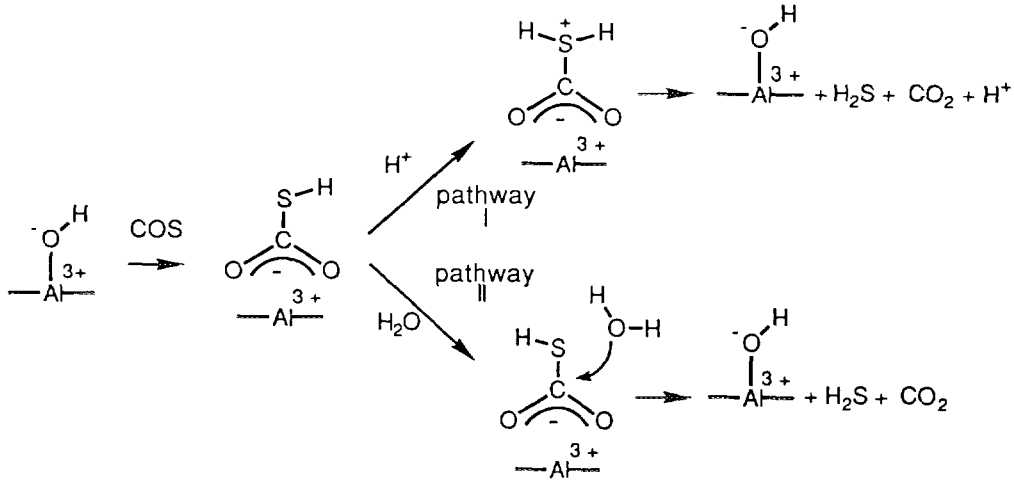

We consider that the latter pathway should be retained because COS hydrolysis proceeds very readily on sodium aluminate (3), a surface without Brønsted acidity.

The experiment carried out at 200 K shows that HTC species formation occurs at this temperature. We also note the presence of physisorbed CO_2 without formation of HC species. The latter are thus not reaction intermediates but result from the readsorption of CO_2 at higher temperatures.

C. Quantum Chemistry Calculations

Information obtained on the COS hydrolysis mechanism on an alumina substrate indicates that the initial chemisorption of COS on the OH base site of alumina takes place via a physisorbed phase through an orientation to maximize COS polarization via a HTC species (Fig. 6).

In the gas phase, the initial OH^- attack would be rate limiting compared with the hydrolysis step. The reverse is shown to be true for the OH-base-catalyzed reaction on an alumina surface.

The pathway mentioned above is shown to be energetically more favorable than chemisorption via the sulfur atom, mainly due to the weakness of the Al–S bond. Furthermore, this step is very specifically catalyzed with a gain of some 209 kJ/mol compared with a homogeneous alkaline hydrolysis.

One result of this catalytic effect is that the subsequent hydrolysis step becomes rate limiting and depends on the presence of a source of H_2O. In the absence of water the HTC species remains *in situ*. The hydrolysis step has been shown to proceed in a concerted process via a nearly regular hexagonal cyclic transition state (Fig. 7a). The HOH angle in the water molecule, for example, widens from an equilibrium gas-phase value of 104.5° to just over 119°. The accompanying activation barrier is 158.4 kJ/

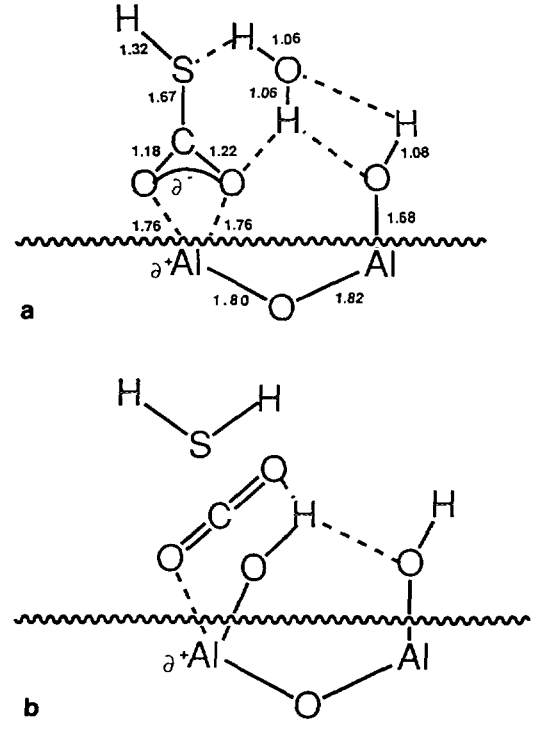

FIG. 7. COS hydrolysis mechanism established by quantum chemical calculations (in-plane projection, distances in Ångstroms). (a) Transition state after H_2O attack, (b) product formation.

mol, as compared with the lower barrier of 130.4 for initial HTC species formation. We obtain as products CO_2 and hydrogen sulfide, with the active site of the alumina surface being restored as it was initially (Fig. 7b). The reverse reaction of chemisorbed CO_2 with hydrogen sulfide has been shown to occur readily with a barrier of similar height leading to the same HTC species as the reaction intermediate.

CONCLUSION

The results observed by IR spectroscopy show that monodentate hydroxyls of alumina are involved in base-catalyzed COS hydrolysis. The first step is hydrogen thiocarbonate species formation for which there is ample spectroscopic evidence. These results served as the starting point of quantum chemistry calculations which provided additional information on the pathway followed by the hydrolysis mechanism. This is a good example of the complementarity afforded by infrared spectroscopy and quantum chemistry calculations in studies on specific reaction mechanisms in heterogeneous catalysis.

REFERENCES

1. Dupin, T., and Voirin, R., *Hydrocarbon Process.*, 189 (1982).
2. Namba, S., and Shiba, T., *Wogyo Wogake Zanki* **71,** 93 (1968).
3. Zdražil, M., *Chem.* Prumysl. Roc., 11 (1974).
4. George, Z. M., *J. Catal.* **32,** 261 (1974).
5. George, Z. M., *J. Catal.* **35,** 218 (1974).
6. Akimoto, M., and Dalla Lana, I. G., *J. Catal.* **62,** 84 (1980).
7. Fiedorow, R., Leaute, R., and Dalla Lana, I. G., *J. Catal.* **85,** 339 (1984).
8. Bachelier, J., Aboulayt, A., Lavalley, J. C., Legendre, O., and Luck, F., *Catal. Today* **17,** 55 (1993).
9. Lavalley, J. C., Aboulayt, K., Lion, M., Bachelier, J., Hebrard, J., and Luck, F., *Prepr. Div. Petrol. Chem. Symp.* **36,** 43 (1991).
10. Nortier, P., Fourre, P., Mohammed Saad, A. B., Saur, O., and Lavalley, J. C., *Appl. Catal.* **61,** 141 (1990).
11. GEOMOS: Rinaldi, D., Hoggan, P. E., and Cartier, A., Quantum Chemistry Program Exchange, Bloomington, IN, Program No. 584 (1989).
12. Hoggan, P. E., D.Sc. Thesis, Nancy (1991).
13. Hoggan, P. E., *Proc. 7th Int. Conference Quantum Chem., Int. J. Quantum Chem.*, 203 (1991).
14. Hoggan, P. E., Bensitel, M., and Lavalley, J. C., *J. Mol. Struct.* **320,** 49 (1994).
15. Hoggan, P. E., and Rinaldi, D., *Theor. Chem. Acta* **72,** 467 (1987).
16. Morterra, C., Zecchina, A., Coluccia, S., and Chiorino, A., *J. Chem. Soc. Faraday Trans. 1* **73,** 1544 (1977).
17. Parkyns, N. D., *J. Phys. Chem.* **75,** 526 (1971).
18. Saur, O., Bensitel, M., Mohammed Saad, A. B., Lavalley, J. C., Tripp, C. P., and Morrow, B. A., *J. Catal.* **99,** 104 (1986).
19. Lavalley, J. C., *Trends Phys. Chem.* **2,** 305 (1991).
20. Travert, J., Chevreau, T., Lamotte, J., Saur, O., and Lavalley, J. C., *J. Chem. Soc. Chem. Commun.*, 146 (1979).
21. Lavalley, J. C., Mohammed Saad, A. B., Tripp, C. P., and Morrow, B. A., *J. Phys. Chem.* **90,** 980 (1986).
22. Saur, O., Chevreau, T., Lamotte, J., Travert, J., and Lavalley, J. C., *J. Chem. Soc., Faraday Trans. 1* **77,** 427 (1981).
23. Lavalley, J. C., Travert, J., Laroche, D., and Saur, O., *C. R. Acad. Sci. Paris C* **285,** 385 (1977).